Chemical Physics 532 (2020) 110680

Contents lists available at ScienceDirect

Chemical Physics

journal homepage: www.elsevier.com/locate/chemphys

Periodic F-defects on the MgO surface as potential single-defect catalysts with non-linear optical properties

Maksim Kulichenko[a], Nikita Fedik[a,b], Dmitry Steglenko[b], Ruslan M. Minyaev[b], Vladimir I. Minkin[b], Alexander I. Boldyrev[a,b,*]

[a] Department of Chemistry and Biochemistry, Utah State University, Logan, UT 84322, USA
[b] Institute of Physical and Organic Chemistry, Southern Federal University, Rostov-on-Don 344090, Russia

ARTICLE INFO

Keywords:
MgO
Surface defects
Single-atom catalysis
Non-linear optics
Bonding
Electride

ABSTRACT

Single-atom catalysis is the ultimate approach in catalysis science which implies the utilization of a catalyst is as efficient as it gets.

In this paper we suggest a new type of a single-atom (or single-defect) catalyst – MgO with periodic defects on the (0 0 1) surface – which possesses noticeable non-linear optical properties. Periodicity of these defects leads to the significant extensive increase in the activity of a catalyst by growth of the concentration of active sites.

In this work we showed the presence of diffuse electride-like multicenter bonds inside every periodic F-center. We also discovered that MgO with periodic defects on the surface gains non-linear optical properties due to electride-like polarizable bonds inside every defect. And most importantly, such defective structures are stable up to 1500 K opening wide range of applications even in extreme conditions.

We considered both multiple (50% surface defects) and rare defects (12.5% surface defects) which are potential single-defect catalysts similar to ones that are reffered as single-atom catalysts.

1. Introduction

From the ancient times humanity was driven by the idea that all the Universe is built of diminutive invisible particles and the time completely proved that wild guess. Centuries after we learned how to operate not only molecules but even to work with single atoms. The utilization of atomic precision looks extremely prospective, especially in the field of catalysis because one could not imagine more efficient catalysts than ones in which every atom or almost every is active. Indeed, such species were recently reported, and single-atom catalysts opened a new frontier in the catalytic science [1–10]. Conventional heterogeneous catalysts are essential to many important industrial chemical processes, but their efficiency is extremely low on a per metal atom basis because only active-site atoms on the surface are involved. Therefore, catalysts with single-atom distribution on the surface are extremely needed to maximize atom activity, but design and fabrication of them is challenging. Recent works report [1–10] on the synthesis of single-atom catalysts that consist of only isolated single catalyst atoms anchored to the surfaces of nanocrystallites. Such single-atom catalysts have extremely high efficiency and show excellent stability and high activity.

At the same time, magnesium oxide is a well-known catalyst [11–20] and supporting surface of catalytic nanoparticles [21–27] for many reactions. Highly reactive defect sites at the surface are mostly responsible for the catalytic activity of this metal oxide [28]. Recently Popov et al. [29] showed that F-center defects – defects with oxygen atom missing – contain doubly occupied electron orbital which can be interpreted as 5-centered bond. These excess electrons can be transferred to the particle or molecule making mentioned F-centers promising catalytic sites on the surface. Interestingly, these 5-centered bonds can be classified as electrides – extraordinary compounds in which electrons are localized in space distinct from atoms and act like anions. There is a number of investigations where electrides were proven to be efficient catalysts and electron conveyors [30–36]. Moreover, electrides are capable of boosting nitrogen dissociation which facilitates the process of ammonia synthesis [30–35]. In addition, many recent theoretical works are devoted to the investigation of molecular electrides, [37–39] and one of them is represented by a defective unitcell of MgO – Mg_4O_3 [40].

Recently we showed that this defective unit cell Mg_4O_3 possesses diffuse electride orbital which is responsible for significant non-linear optical (NLO) properties of this molecule. NLO materials attract

* Corresponding author at: Department of Chemistry and Biochemistry, Utah State University, Logan, UT 84322, USA.
E-mail address: a.i.boldyrev@usu.edu (A.I. Boldyrev).

https://doi.org/10.1016/j.chemphys.2020.110680
Received 13 December 2019; Received in revised form 14 January 2020; Accepted 15 January 2020
Available online 20 January 2020
0301-0104/

significant interest because of their wide applications in optical computing, optical communication, laser devices, and dynamic image processing [41–49].

In the present work we would like to focus on catalytic and non-linear properties of MgO crystalline surface (001) with superstructures built out of F-centers containing diffuse electride-like bonds. These bonds consist of electrons coming from Mg atoms and the entire system remains neutral since neutral oxygen atoms are detached from the surface. We made these defects in a periodic fashion with different types of periodicity – multiple and rare. Being periodic, these sites extensively increase the catalytic activity and non-linear optical response of the MgO surface which is of great importance for efficient catalyst utilization and second harmonic generation (SHG).

Using quantum chemistry tools we managed to show that magnesium oxide with periodic voids missing oxygen atoms on the surface is a stable structure even at the temperature of 1500 K. And most importantly, these voids possess electride-like doubly occupied diffuse bonds which makes them potential candidates for single-atom catalytic sites. In the science of heterogeneous catalysis, many efforts were devoted toward the downsizing the catalytic sites and one may consider these sites on MgO surface as the smallest possible single-defect catalyst sites (or single electron pair site since there are actually two electrons in every void). At the same time, possessing diffuse polarizable bonds, these sites are responsible for the non-linear optical response. Fast development of modern experimental methods, including individual atom removal techniques, gives us hope that creation of such species is just a matter of time.

2. Computational methods

Geometry optimization of the MgO crystalline with periodic F-centers was performed within the DFT approach using the generalized gradient approximation (GGA) with the Perdew-Burke-Ernzerhof exchange–correlation functional revised for solids (PBEsol) [48] and the projected augmented wave approach, as implemented in the Vienna Ab-initio Simulation Package (VASP) [50]. The following lattice constants were used for the pristine MgO unit cell (Fig. 1): a = b = c = 4.16 Å.

The non-stoichiometric MgO with multiple defects was modeled as 1x1x2.5 (six layers) MgO pristine supercell (Fig. 1) with one O atom removed from the surface, i.e., every second oxygen is missing on the surface (Fig. 1). For the MgO slab a vacuum gap of 15 Å was added in the z direction to eliminate interactions between cells. In this case, the lattice parameters are a = b = 4.16 Å, c = 20 Å. The Brillouin zone was sampled with a 13 × 13 × 1 Γ-centered Monkhorst-Pack [51] k-point grid.

The non-stoichiometric MgO with rare defects was modeled as 2 × 2 × 2.5 MgO pristine supercell with one O atom removed from the surface, i.e., every eighth oxygen is missing on the surface (Fig. 1). The same vacuum gap was added. In this case, the lattice parameters are a = b = 8.31 Å, c = 20 Å. The Brillouin zone was sampled with a 6 × 6 × 1 Monkhorst-Pack k-point grid.

Large kinetic energy cutoff of 450.0 eV was used alongside with the tight electronic convergence criteria of 10^{-8} eV and forces threshold of 10^{-4} eV/Å for optimization within quasi-Newton ionic relaxation algorithm. Since MgO is known as insulator, we used Gaussian smearing for determining partial occupancies of orbitals and converged occupation threshold of 0.05.

Periodic NBO [52,53] and SSAdNDP [54–57] calculations were performed using the same parameters within VASP. Periodic NBO, like the standard NBO code, allows the recognition of 1c-2e bonds (lone pairs) and 2c-2e bonds (2-centered 2-electron bonds). SSAdNDP code, which is an extension of original AdNDP [58–63] for solid state calculations, enables the identification of multicenter delocalized chemical bonds (nc-2e, n > 2). Both NBO and AdNDP codes work within the concept of occupation numbers (ON), which represent the amount of electron density localized in a certain bond. The closer these values to 2, the more trustworthy bonding picture is. User-Directed Search procedure implemented in SSAdNDP (UD-SSAdNDP) enables solving tricky bonding cases. Guidelines to UD search and comprehensively described examples can be found in supplementary information of the following references [64,65].

We chose the cc-pVTZ [66] basis set for representing the projected PW so, electron density matrix used for SSAdNDP calculations is in precise agreement with the initial PW results.

Phonon spectra (Fig. 2) calculations were performed using finite displacements method implemented in Phonopy code [67].

Molecular dynamics (MD) simulations were performed within VASP software using 1 fs time step and 6000 steps. Temperature control was performed using Nose-Hoover method [68].

The work functions were calculated using dipole interaction corrections along z-directions corresponding to the vacuum gap.

The NLO properties of defective MgO surface were explored by ABINIT [69] software within Random-Phase Approximation (RPA) [70].

The electron pair inside the F-center is highly diffuse and, hence, more “flexible”. Therefore, even week electric field can cause high polarization which is no longer linear against the applied field. In this work we investigate the second order polarizability which is usually referred as first hyperpolarizability. This property is used, for example, for second harmonic generation when two photons of frequency ω cause the emission of the photon with frequency 2ω.

The optical responses are driven by electron state transitions, excitonic effects, and phonon effects. The electron state transitions have the biggest contribution and, hence, RPA usually gives reasonable picture of NLO spectra. The expressions in Eqs. (46), (49), and (50) in reference [70] give linear and second-order nonlinear susceptibilities within the RPA. Position matrix elements r_{mn} are determined by response wavefunctions which are computed by density functional perturbation theory [71]. Since LDA and GGA approximations tend to underestimate band gaps [72], we used the G0W0 [73,74] method to calculate defective MgO quasiparticle band structure. The G0W0 corrected gap was used as scissor shift to calculate the nonlinear optical properties. To get reasonable optical spectrum, a large number of bands (280) and dense sampling of k-points (24 × 24 × 1) are used for NLO response calculations. Kinetic energy cutoff of 20 Ha was chosen. To be unbiased on the geometry used, we performed structural optimization within ABINIT as well. The geometry obtained via Broyden-Fletcher-Goldfarb-Shanno optimization algorithm [75] is essentially the same as used in the abovementioned calculations. LDA-PAW pseudopotentials provided by ABINIT database [76,77] were used.

3. Results and discussion

3.1. Electronic properties

Although the symmetry of a system with multiple defects decreases after the removal of oxygen atom, the lattice still possesses a rotational axis along z direction (4) and reflection planes (m) containing this axis. That is why we did not observe any displacements in comparison with salt structure: Mg-O bond length is 2.08 Å in every layer.

The same situation can be observed in a system with rare defects, though some Mg-O distances differ by the value of 0.07 A. We consider such differences as negligible and not deserving a special discussion.

To understand the bonding nature of both systems we performed periodic NBO and SSAdNDP analysis. As for multiple defects case, the unit cell contains 12 Mg atoms and 11 O atoms giving us 45 valence pairs in sum. The bonding analysis gave us quite classical picture for 44 of them: they are distributed as s, p_x, p_y and p_z lone pairs (LPs) on oxygen atoms with ONs of 1.77–1.90 |e| supporting the conventional ionic $Mg^{2+}O^{2-}$ representation. Using Direct Search implemented in SSAdNDP code we revealed that the remaining valence pair could not be localized in Lewis-like fashion. It is delocalized over five Mg atoms

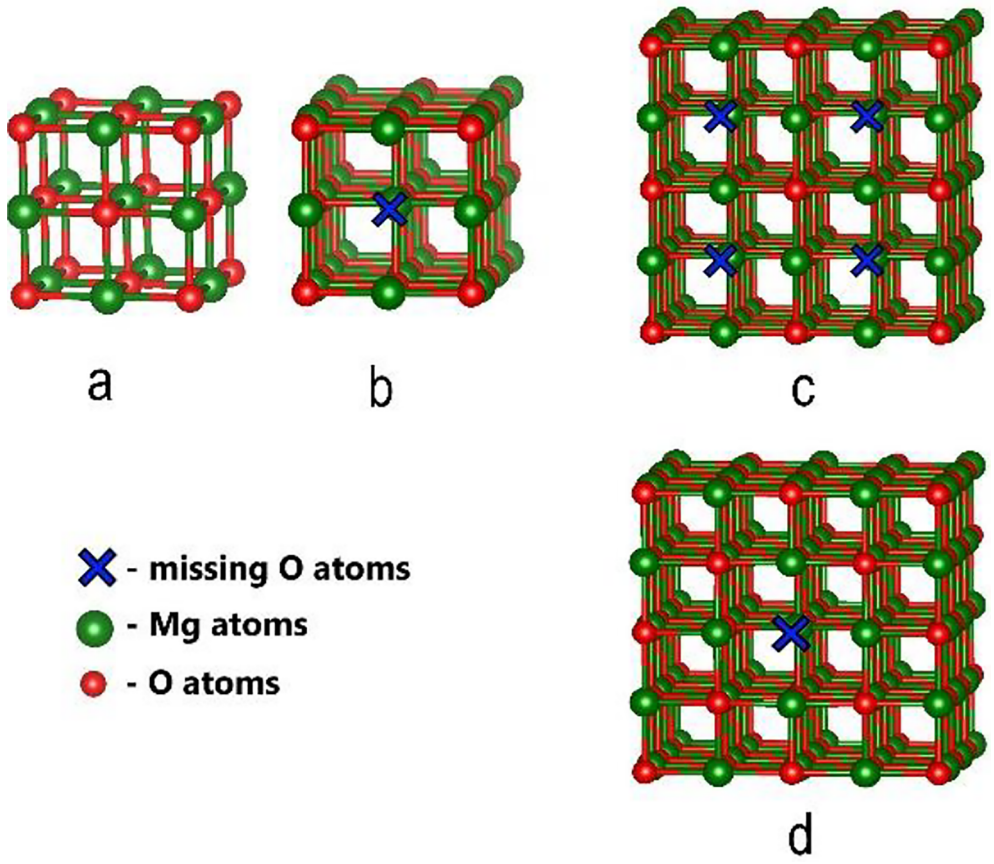

Fig. 1. a: pristine MgO unitcell. b: unitcell of MgO slab with every second surface oxygen atom removed. c: 2x2x1 supercell of slab with the same defect superstructure. d: 1x1x1 supercell slab with every eight surface O removed.

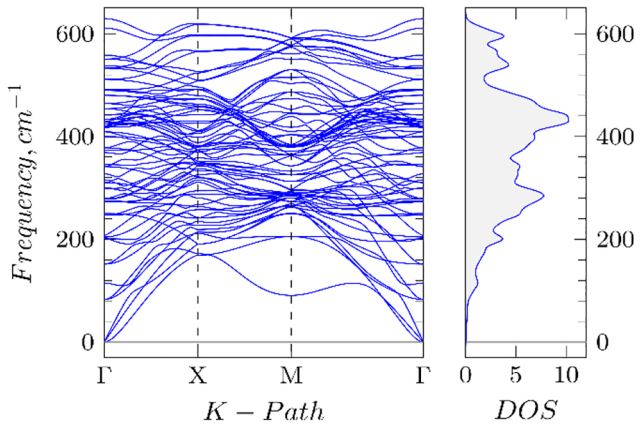

Fig. 2. Phonon spectrum of MgO slab with multiple defects.

around the surface defect like σ bond with the ON = 1.84 |e| (Fig. 3). When including Mg atoms from both 1st and 2nd coordination spheres (9c-2e bond), the ON slightly increases up to 1.90 |e|.

The same technique was used for bonding analysis in slab with rare defects and approximately the same ONs (1.83 |e| for 5c-2e and 1.90 |e| for 9c-2e bonds) were obtained (Fig. 3).

Band structure analysis (Fig. 4) of slab structures with and without defects revealed that the removal of oxygen atom from the surface induces the noticeably higher in energy band which, in turn, significantly lowers the optical surface band gap from 3.1 to 1.6 eV. However, DFT calculations usually underestimate band gaps. By means of more sophisticated G0W0 approximation we obtained corrected band gap of 5.2 eV for pristine slab and 2.9 eV for the periodically defective slab. The work function decreased from 5.0 (which is quite close to experimental values)[78] to 3.3 eV, according to our calculations. These observations indicate the increase in reactivity of the system upon the removal of every second oxygen from the surface.

Calculation of pristine bulk MgO within the same approach including G0W0 corrections gave band gap of 7.10 eV which by about 10% less than experimental value of 7.77 eV [79], indicating the reliability of our level of theory.

One may set a fair point that these results could be dependent on the functional used. Here we refer to the work of Popov et al. in which they tested PBE [80] and HSE06 [81,82] functionals for the system similar with ours and obtained essentially the same results for both levels of theory.

As we mentioned above, this crystalline with periodic defects could be a promising non-linear optical material and catalyst with single-defect (or single electron pair) sites. Therefore, to make its utilization possible, we must show the structure is stable at least at room temperature. Actually, the results are much more promising: molecular dynamics calculations of multiple defects case indicate that the structure is unchanged at least up to 1500 K which is clearly reflected in the pair correlation function graph (Fig. 5). This fact allows the application of defective MgO even in extremely exothermic chemical processes and high-temperature reactors.

3.2. Optical properties

First principle calculations have been successfully used to obtain different properties of bulk semiconductors, such as linear and non-linear optical properties (just to name few [70,83–86]).

In this section we provide calculated optical properties of MgO with multiple defects on the surface. According to LDA-DFT level of theory

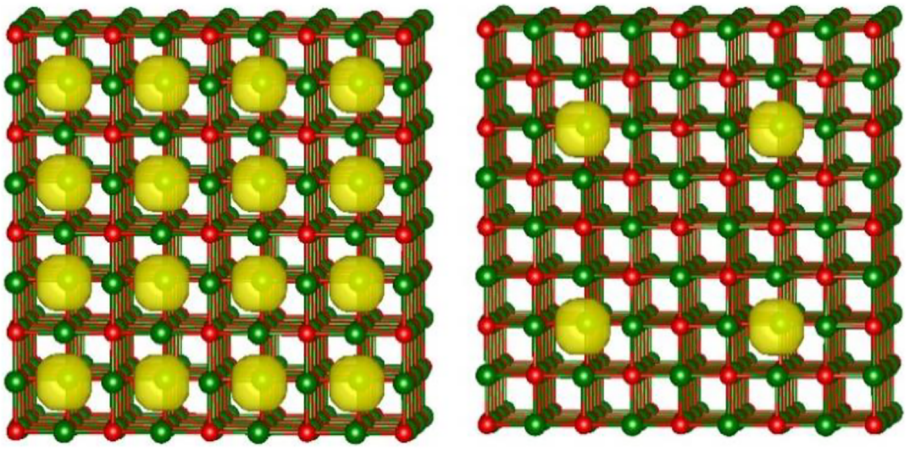

Fig. 3. Left: bonding analysis of MgO slab with multiple defects. Right: bonding analysis of MgO slab with rare defects.

via ABINIT, the calculated minimum optical surface band gap E_g = 1.6 eV. Using G0W0 corrections, we obtained the value of 3.1 eV which is used in optical spectrum calculations by means of scissor shift. Although in this study we are focused on non-linear response, firstly, we would suggest to take a brief look at linear susceptibility spectrum for the optical picture to be complete. In Figs. 6 and 7 we present imaginary and real parts of complex dielectric functions ε_{11} and ε_{33} for MgO slab with multiple defects. We do not perform any detailed assignments of peaks. According to the low energy limit, static dielectric constants $\varepsilon_1(0)$ and $\varepsilon_3(0)$ are 2.95 and 2.61 respectively. Definitely, the highest peak of ε_{11} near 3.1 eV comes from transition from the highest valence band (HVB) to the lowest conduction band (LCB) near X k-point which corresponds to optical band gap (3.1 eV). The highest peak of ε_{33} likely comes from transition between HVB and LCB at Γ k-point which is 4.1 eV after being scissor corrected.

Among all tensor components of second-order optical susceptibility, two independent non-zero components $X^{(2)}_{333}$ (2ω, ω, ω) and $X^{(2)}_{311}$ (2ω,ω, ω) are calculated in this work. In Fig. 8 we present different contributions to the imaginary part $ImX^{(2)}_{333}$ (2ω,ω, ω) of $X^{(2)}_{333}$ (2ω, ω, ω). The real part can be obtained using the Kramers–Kronig relations.

As we can see, all components of imaginary part of the second-order susceptibility are vanishing as energy goes to zero. However, starting with ~2 eV we can observe many peaks and significant non-zero absolute values. The 2ω terms start contributing to the total value at energies about $1/2E_g$ and are completely dominating at low energy regions below ~4.2 eV. Though inter and intraband components have

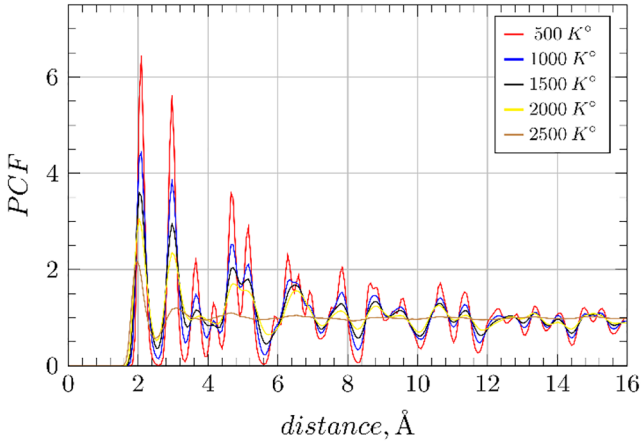

Fig. 5. Pair correlation function of MgO slab with multiple defects.

opposite signs and partially cancel each other, they result in significant peaks of the absolute value. At the same time, the 1ω contributions become non-zero at energies above E_g and the region between 4.6 eV and 5.2 eV is mostly dominated by 1ω terms. In higher energy region all terms mostly cancel each other resulting in insignificant total values of $ImX^{(2)}_{333}$ (2ω, ω, ω). More detailed examination of the second-order susceptibility spectrum is essentially complicated due to the unobvious resonances of 2ω and 1ω terms.

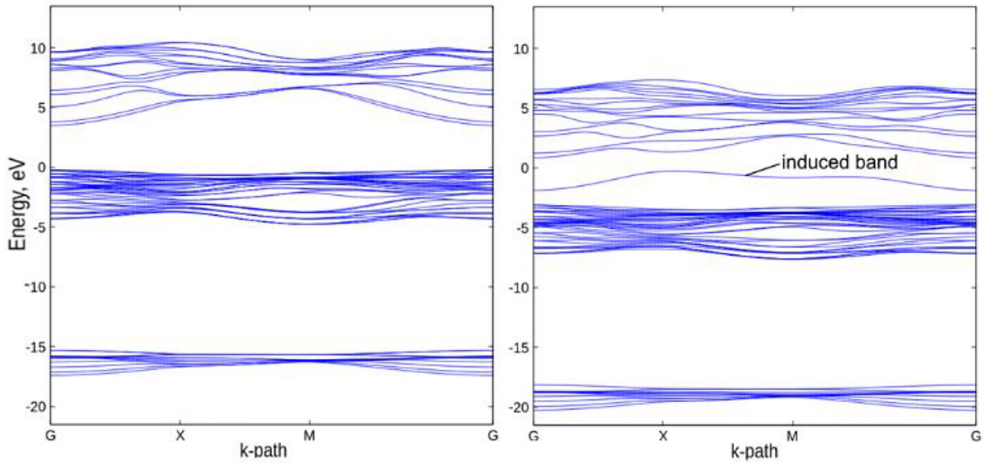

Fig. 4. Left: bandstructure of MgO slab without defects. Right: bandstructure of MgO with multiple F-defect. Fermi-levels are set as zeroes. In both cases vacuum gap is added in z-direction.

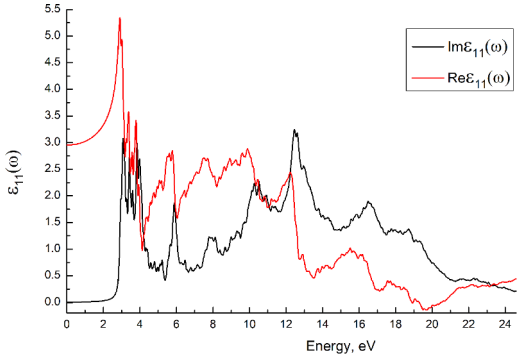

Fig. 6. Imaginary and real parts of optical dielectric function $\varepsilon_{\perp}$ of MgO slab with every second oxygen removed from the surface.

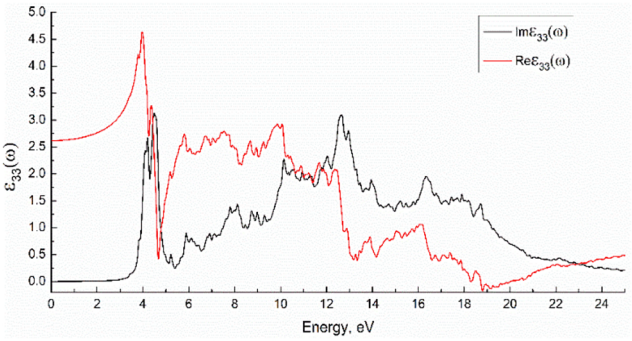

Fig. 7. Imaginary and real parts of optical dielectric function $\varepsilon_{\parallel}$ of MgO slab with every second oxygen removed from the surface.

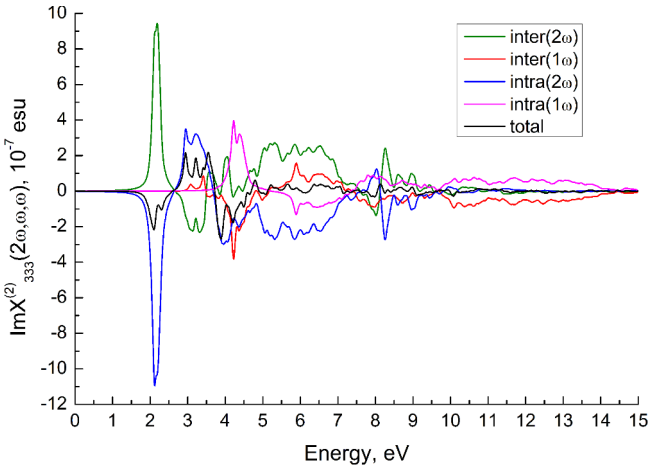

Fig. 8. Calculated $ImX^{(2)}_{333}$ (2ω, ω, ω) spectra with the intra-(2ω)/(1ω) and inter-(2ω)/(1ω) band contributions of MgO slab with every second oxygen removed from the surface.

Next we present the frequency-dependent spectrum of the absolute value of $X^{(2)}_{333}$ (2ω, ω, ω) (Fig. 9). Although $|X^{(2)}_{333}(0)|$ is small (0.04 10^{-7} esu) at static frequency limit, the most pronounced NLO properties are in low energy region between 2.0 and 5.2 eV with peaks of magnitude up to 3.5 10^{-7} esu.

Imaginary part of 311 second-order susceptibility tensor component $ImX^{(2)}_{311}$ (2ω, ω, ω) (Fig. 10) has 2ω contributions mostly dominating from 1.0 to 2.8 eV with amplitude significantly higher than in 333 component resulting in twice higher amplitude of absolute value of imaginary part. Above 5.8 eV all components tend to cancel each other resulting in almost zero absolute values of imaginary part.

The absolute value of 331 second-order susceptibility tensor

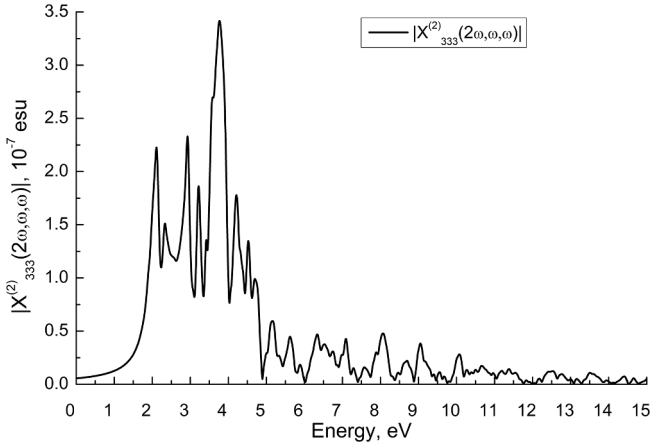

Fig. 9. Absolute value of the second-order nonlinear susceptibility $X^{(2)}_{333}$ (2ω, ω, ω) of MgO with multiple defects.

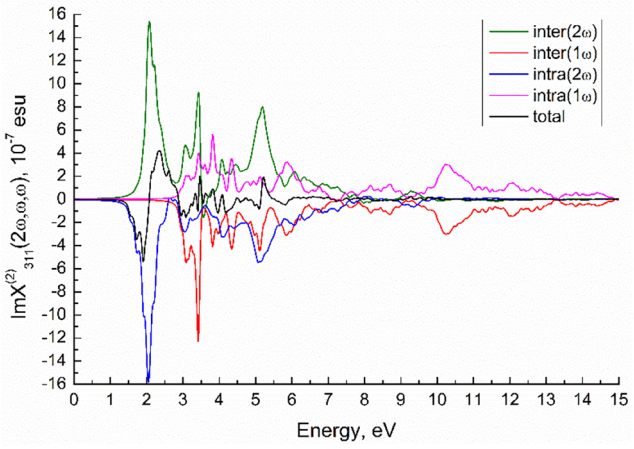

Fig. 10. Calculated $ImX^{(2)}_{311}$ (2ω, ω, ω) spectra with the intra-(2ω)/(1ω) and inter-(2ω)/(1ω) band contributions of MgO slab with every second oxygen removed from the surface.

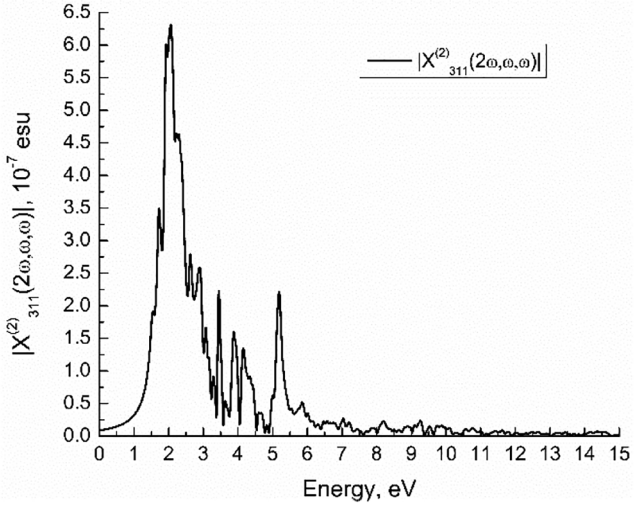

Fig. 11. Absolute value of the second-order nonlinear susceptibility $X^{(2)}_{311}$ (2ω, ω, ω) of MgO with multiple defects.

component $|X^{(2)}_{311}$ (2ω, ω, ω)| (Fig. 11) also has twice higher peak magnitude than $|X^{(2)}_{333}$ (2ω, ω, ω)|. Noticeably, the static limit value is more than twice bigger as well being 0.09 10^{-7} esu. According to the graph, the most pronounced NLO properties are supposed to be

between 1.0 and 6.0 eV.

We also would like to point out that the first- and second-order susceptibilities are inversely dependent on the volume of a crystal ($\chi^{(2)}_{333}$ (2ω, ω, ω) ~ 1/ Ω). Since the slab of defective MgO is modelled using big vacuum gap of 15 Å, we expect the real values to be at least twice higher than calculated in this work. Anyway, we believe our calculations qualitatively prove that periodically defective MgO possesses noticeable non-linear properties in low energy region.

The inclusion of excitonic effects and phonon-assisted processes, which are extremely computationally demanding, could somehow change positions and mutual magnitude of peaks, however, it should not change significantly the average magnitude and the general picture. We believe RPA is completely enough for purposes of this work. Moreover, there is a number of work where RPA calculations are in good agreement with experimental data [83,86–88].

We believe that modern equipment enables the creation of abovementioned defects at low costs. Besides widely known radiation damage techniques, recently a new method of individual atoms manipulation [89–93] attracts lots of attention giving as a hope of soon fabrication of the designed material.

4. Conclusions

Using electronic structure analysis, we showed that a simple textbook compound MgO still may surprise with its structural and electronic properties.

First, let us summarize commonly known facts. Every MgO crystalline naturally has randomly spaced F-centers on its surface resulted from the removal of oxygen atoms. Bonding analysis of these defects reveals doubly occupied 5c-2e bonds in the voids. Such diffuse electron pairs localized in places distinct from atomic positions are known as electride phases of materials and have already found a plenty of applications including catalysts, electron conveyors, and non-linear optics. It is known that MgO is widely-used as a catalyst and supporting surface, and extremely reactive defect sites at the MgO surface are mostly responsible for such high catalytic activity.

In this work, following the abovementioned facts, we proposed the idea of periodic defects on the (001) MgO surface. The periodicity of these defects extensively increases the catalytic activity of species by multiplication of active sites number. Noticeably, such geometry manipulations do not affect the stability of the structure. We studied both multiple periodic defects (every second oxygen atom is removed from the surface) and rare periodic defects (every eighth oxygen is removed). Phonon spectrum stability tests did not reveal any imaginary frequencies. Moreover, molecular dynamics simulations indicate that the structure with electron pairs on the surface is kept even at the temperature of 1500 K which enables the application of defective MgO in high temperature conditions.

In addition, we showed that MgO crystalline with every second oxygen removed from the surface is a promising material for non-linear optical applications. Using Random-Phase Approximation in the context of DFT, it was predicted that this defective crystal has noticeable non-linear optical properties in low energy region between 1.0 and 6.0 eV. This result indicates that pristine MgO, which has the center of inversion and does not exhibit any nonlinearity, can be tuned by means of defects to be used for second-harmonic generation.

No doubt, up-to-date methods, including radiation damage and individual atom removal techniques, can easily handle the issue of creating the mentioned periodic F-centers on the surface. We refer to these new surface materials as single-defect (F1) catalysts which are similar to what community calls the single-atom catalysts. We hope this approach can be used to design other single-defect catalysts with missing oxygen atoms in oxides of main group and transition metals as well. Many of them may also exhibit NLO properties induced by defects and the loss of the inversion center.

CRediT authorship contribution statement

Maksim Kulichenko: Writing - original draft, Methodology, Formal analysis, Visualization. **Nikita Fedik:** Writing - review & editing, Methodology, Formal analysis. **Dmitry Steglenko:** Writing - review & editing, Methodology, Software, Formal analysis, Visualization. **Ruslan M. Minyaev:** Writing - review & editing, Conceptualization, Resources, Funding acquisition. **Vladimir I. Minkin:** Writing - review & editing, Conceptualization, Resources, Funding acquisition. **Alexander I. Boldyrev:** Writing - review & editing, Conceptualization, Methodology, Validation, Investigation, Resources, Supervision, Project administration, Funding acquisition.

Declaration of Competing Interest

The authors declare that they have no known competing financial interests or personal relationships that could have appeared to influence the work reported in this paper.

Acknowledgements

The work was supported by the Russian Government grant by decree N 220 (agreement № 14.Y26.31.0016) and by the USA National Science Foundation (grant CHEM-1664379) to AIB. The support and resources from the Centre for High Performance Computing at the University of Utah are gratefully acknowledged.

References

[1] B. Qiao, A. Wang, X. Yang, L.F. Allard, Z. Jiang, Y. Cui, J. Liu, J. Li, T. Zhang, Single-atom catalysis of CO oxidation using Pt1/FeOx, Nat. Chem. 3 (2011) 634–641, https://doi.org/10.1038/nchem.1095.

[2] X.-F. Yang, A. Wang, B. Qiao, J. Li, J. Liu, T. Zhang, Single-Atom Catalysts: A New Frontier in Heterogeneous Catalysis, Acc. Chem. Res. 46 (2013) 1740–1748, https://doi.org/10.1021/ar300361m.

[3] A. Wang, J. Li, T. Zhang, Heterogeneous single-atom catalysis, Nat. Rev. Chem. 2 (2018) 65–81, https://doi.org/10.1038/s41570-018-0010-1.

[4] J. Lin, A. Wang, B. Qiao, X. Liu, X. Yang, X. Wang, J. Liang, J. Li, J. Liu, T. Zhang, Remarkable Performance of Ir1/FeOx Single-Atom Catalyst in Water Gas Shift Reaction, J. Am. Chem. Soc. 135 (2013) 15314–15317, https://doi.org/10.1021/ja408574m.

[5] X. Li, X. Yang, Y. Huang, T. Zhang, B. Liu, Supported Noble-Metal Single Atoms for Heterogeneous Catalysis, Adv. Mater. (2019) 1902031, https://doi.org/10.1002/adma.201902031.

[6] W. Cao, L. Lin, H. Qi, Q. He, Z. Wu, A. Wang, W. Luo, T. Zhang, In-situ synthesis of single-atom Ir by utilizing metal-organic frameworks: An acid-resistant catalyst for hydrogenation of levulinic acid to γ-valerolactone, J. Catal. 373 (2019) 161–172, https://doi.org/10.1016/j.jcat.2019.03.035.

[7] X. Shao, X. Yang, J. Xu, S. Liu, S. Miao, X. Liu, X. Su, H. Duan, Y. Huang, T. Zhang, Iridium Single-Atom Catalyst Performing a Quasi-homogeneous Hydrogenation Transformation of CO_2 to Formate, Chem. 5 (2019) 693–705, https://doi.org/10.1016/j.chempr.2018.12.014.

[8] B. Qiao, J. Liu, Y.-G. Wang, Q. Lin, X. Liu, A. Wang, J. Li, T. Zhang, J. Liu, Highly Efficient Catalysis of Preferential Oxidation of CO in H_2-Rich Stream by Gold Single-Atom Catalysts, ACS Catal. 5 (2015) 6249–6254, https://doi.org/10.1021/acscatal.5b01114.

[9] Y.-Q. Su, Y. Wang, J.-X. Liu, I.A.W. Filot, K. Alexopoulos, L. Zhang, V. Muravev, B. Zijlstra, D.G. Vlachos, E.J.M. Hensen, Theoretical Approach To Predict the Stability of Supported Single-Atom Catalysts, ACS Catal. 9 (2019) 3289–3297, https://doi.org/10.1021/acscatal.9b00252.

[10] C. Choi, S. Back, N.-Y. Kim, J. Lim, Y.-H. Kim, Y. Jung, Suppression of Hydrogen Evolution Reaction in Electrochemical N_2 Reduction Using Single-Atom Catalysts: A Computational Guideline, ACS Catal. 8 (2018) 7517–7525, https://doi.org/10.1021/acscatal.8b00905.

[11] X.D. Peng, D.A. Richards, P.C. Stair, Surface composition and reactivity of lithium-doped magnesium oxide catalysts for oxidative coupling of methane, J. Catal. 121 (1990) 99–109, https://doi.org/10.1016/0021-9517(90)90220-E.

[12] G. Szöllösi, M. Bartók, Hydrogenation of unsaturated ketones: selective catalytic transfer hydrogenation of 5-hexen-2-one over MgO, J. Mol. Catal. A Chem. 148 (1999) 265–273, https://doi.org/10.1016/S1381-1169(99)00159-4.

[13] M.A. Aramendía, V. Borau, C. Jiménez, J.M. Marinas, F.J. Romero, Vapour-Phase Reaction of Acetophenone with Methanol or Dimethyl Carbonate on Magnesium Oxide and Magnesium Phosphates, J. Catal. 183 (1999) 119–127, https://doi.org/10.1006/jcat.1998.2360.

[14] S. Kuś, M. Otremba, A. Tórz, M. Taniewski, The effect of gas atmosphere used in the calcination of MgO on its basicity and catalytic performance in oxidative coupling of methane, Appl. Catal. A Gen. 230 (2002) 263–270, https://doi.org/10.1016/

S0926-860X(02)00039-X.
[15] M.T. Drexler, M.D. Amiridis, The effect of solvents on the heterogeneous synthesis of flavanone over MgO, J. Catal. 214 (2003) 136–145, https://doi.org/10.1016/S0021-9517(02)00013-1.
[16] R. López-Asensio, P.C. Jiménez Gómez, C. García Sancho, R. Moreno-Tost, A.J. Cecilia, P. Maireles-Torres, Influence of Structure-modifying Agents in the Synthesis of Zr-doped SBA-15 Silica and Their Use as Catalysts in the Furfural Hydrogenation to Obtain High Value-added Products through the Meerwein-Ponndorf-Verley Reduction, Int. J. Mol. Sci. 20 (2019), https://doi.org/10.3390/ijms20040828.
[17] M. Di Serio, M. Ledda, M. Cozzolino, G. Minutillo, R. Tesser, E. Santacesaria, Transesterification of Soybean Oil to Biodiesel by Using Heterogeneous Basic Catalysts, Ind. Eng. Chem. Res. 45 (2006) 3009–3014, https://doi.org/10.1021/ie051402o.
[18] M. Di Serio, R. Tesser, L. Pengmei, E. Santacesaria, Heterogeneous Catalysts for Biodiesel Production, Energy Fuels 22 (2008) 207–217, https://doi.org/10.1021/ef700250g.
[19] J.M. Montero, M.A. Isaacs, A.F. Lee, J.M. Lynam, K. Wilson, The surface chemistry of nanocrystalline MgO catalysts for FAME production: An in situ XPS study of H_2O, CH_3OH and CH_3OAc adsorption, Surf. Sci. 646 (2016) 170–178, https://doi.org/10.1016/j.susc.2015.07.011.
[20] Y.C. Sharma, B. Singh, J. Korstad, Latest developments on application of heterogenous basic catalysts for an efficient and eco friendly synthesis of biodiesel: A review, Fuel 90 (2011) 1309–1324, https://doi.org/10.1016/j.fuel.2010.10.015.
[21] L. Ma, M. Melander, T. Weckman, K. Laasonen, J. Akola, CO Oxidation on the $Au_{15}Cu_{15}$ Cluster and the Role of Vacancies in the MgO(100) Support, J. Phys. Chem. C. 120 (2016) 26747–26758, https://doi.org/10.1021/acs.jpcc.6b06876.
[22] L. Shen, J. Dadras, A.N. Alexandrova, Pure and Zn-doped Pt clusters go flat and upright on MgO(100), Phys. Chem. Chem. Phys. 16 (2014) 26436–26442, https://doi.org/10.1039/C4CP01877J.
[23] J. Dadras, L. Shen, A. Alexandrova, Pt–Zn Clusters on Stoichiometric MgO(100) and TiO_2(110): Dramatically Different Sintering Behavior, J. Phys. Chem. C. 119 (2015) 6047–6055, https://doi.org/10.1021/jp512277x.
[24] D. Ricci, A. Bongiorno, G. Pacchioni, U. Landman, Bonding Trends and Dimensionality Crossover of Gold Nanoclusters on Metal-Supported MgO Thin Films, Phys. Rev. Lett. 97 (2006) 36106, https://doi.org/10.1103/PhysRevLett. 97.036106.
[25] B. Yoon, U. Landman, Electric Field Control of Structure, Dimensionality, and Reactivity of Gold Nanoclusters on Metal-Supported MgO Films, Phys. Rev. Lett. 100 (2008) 56102, https://doi.org/10.1103/PhysRevLett. 100.056102.
[26] L.B. Vilhelmsen, B. Hammer, Systematic Study of Au_6 to Au_{12} Gold Clusters on MgO (100) F Centers Using Density-Functional Theory, Phys. Rev. Lett. 108 (2012) 126101, , https://doi.org/10.1103/PhysRevLett. 108.126101.
[27] J. Dadras, E. Jimenez-Izal, A.N. Alexandrova, Alloying Pt Sub-nano-clusters with Boron: Sintering Preventative and Coke Antagonist? ACS Catal. 5 (2015) 5719–5727, https://doi.org/10.1021/acscatal.5b01513.
[28] J.M. Vohs, The surface science of metal oxides. V.E. Henrich, P. A. Cox (Eds.), Cambridge University Press, Cambridge, U.K., 1994, 464 pp., AIChE J. 44 (1998) 502–503. doi:10.1002/aic.690440230.
[29] I.A. Popov, E. Jimenez-Izal, A.N. Alexandrova, A.I. Boldyrev, Multicenter Bonding Effects in Oxygen Vacancy in the Bulk and on the Surface of MgO, J. Phys. Chem. C. 122 (2018) 11933–11937, https://doi.org/10.1021/acs.jpcc.8b03118.
[30] M. Kitano, Y. Inoue, Y. Yamazaki, F. Hayashi, S. Kanbara, S. Matsuishi, T. Yokoyama, S.-W. Kim, M. Hara, H. Hosono, Ammonia synthesis using a stable electride as an electron donor and reversible hydrogen store, Nat. Chem. 4 (2012) 934.
[31] M. Kitano, S. Kanbara, Y. Inoue, N. Kuganathan, P.V. Sushko, T. Yokoyama, M. Hara, H. Hosono, Electride support boosts nitrogen dissociation over ruthenium catalyst and shifts the bottleneck in ammonia synthesis, Nat. Commun. 6 (2015) 6731, https://doi.org/10.1038/ncomms7731.
[32] Y. Inoue, M. Kitano, K. Kishida, H. Abe, Y. Niwa, M. Sasase, Y. Fujita, H. Ishikawa, T. Yokoyama, M. Hara, H. Hosono, Efficient and Stable Ammonia Synthesis by Self-Organized Flat Ru Nanoparticles on Calcium Amide, ACS Catal. 6 (2016) 7577–7584, https://doi.org/10.1021/acscatal.6b01940.
[33] M. Hara, M. Kitano, H. Hosono, Ru-Loaded $C_{12}A_7$:e– Electride as a Catalyst for Ammonia Synthesis, ACS Catal. 7 (2017) 2313–2324, https://doi.org/10.1021/acscatal.6b03357.
[34] J. Wu, Y. Gong, T. Inoshita, D.C. Fredrickson, J. Wang, Y. Lu, M. Kitano, H. Hosono, Tiered Electron Anions in Multiple Voids of LaScSi and Their Applications to Ammonia Synthesis, Adv. Mater. 29 (2017) 1700924, https://doi.org/10.1002/adma.201700924.
[35] M. Kitano, Y. Inoue, M. Sasase, K. Kishida, Y. Kobayashi, K. Nishiyama, T. Tada, S. Kawamura, T. Yokoyama, M. Hara, H. Hosono, Self-organized Ruthenium-Barium Core–Shell Nanoparticles on a Mesoporous Calcium Amide Matrix for Efficient Low-Temperature Ammonia Synthesis, Angew. Chem. Int. Ed. 57 (2018) 2648–2652, https://doi.org/10.1002/anie.201712398.
[36] H. Buchammagari, Y. Toda, M. Hirano, H. Hosono, D. Takeuchi, K. Osakada, Room Temperature-Stable Electride as a Synthetic Organic Reagent: Application to Pinacol Coupling Reaction in Aqueous Media, Org. Lett. 9 (2007) 4287–4289, https://doi.org/10.1021/ol701885p.
[37] V. Postils, M. Garcia-Borràs, M. Solà, J.M. Luis, E. Matito, On the existence and characterization of molecular electrides, Chem. Commun. 51 (2015) 4865–4868, https://doi.org/10.1039/C5CC00215J.
[38] M. Garcia-Borràs, M. Solà, J.M. Luis, B. Kirtman, Electronic and Vibrational Nonlinear Optical Properties of Five Representative Electrides, J. Chem. Theory Comput. 8 (2012) 2688–2697, https://doi.org/10.1021/ct300433q.
[39] O. El-Bakouri, V. Postils, M. Garcia-Borràs, M. Duran, J.M. Luis, S. Calvello, A. Soncini, E. Matito, F. Feixas, M. Solà, Metal Cluster Electrides: A New Type of Molecular Electride with Delocalised Polyattractor Character, Chem.-A Eur. J. 24 (2018) 9853–9859, https://doi.org/10.1002/chem.201800878.
[40] M. Kulichenko, N. Fedik, K.V. Bozhenko, A.I. Boldyrev, Inorganic Molecular Electride Mg_4O_3: Structure, Bonding, and Nonlinear Optical Properties, Chem.-A Eur. J. 25 (2019) 5311–5315, https://doi.org/10.1002/chem.201806372.
[41] H. Hora, Y.R. Shen, The Principles of Nonlinear Optics, John Wiley & Sons, New York, 1984, 576 pages, Laser Part. Beams. 4 (1986) 318–319, https://doi.org/10.1017/S0263034600001889.
[42] D.R. Kanis, M.A. Ratner, T.J. Marks, Design and construction of molecular assemblies with large second-order optical nonlinearities. Quantum chemical aspects, Chem. Rev. 94 (1994) 195–242, https://doi.org/10.1021/cr00025a007.
[43] J.L. Oudar, D.S. Chemla, Hyperpolarizabilities of the nitroanilines and their relations to the excited state dipole moment, J. Chem. Phys. 66 (1977) 2664–2668, https://doi.org/10.1063/1.434213.
[44] B.J. Coe, J. Fielden, S.P. Foxon, I. Asselberghs, K. Clays, B.S. Brunschwig, Two-Dimensional, Pyrazine-Based Nonlinear Optical Chromophores with Ruthenium(II) Ammine Electron Donors, Inorg. Chem. 49 (2010) 10718–10726, https://doi.org/10.1021/ic1019197.
[45] B.J. Coe, Switchable Nonlinear Optical Metallochromophores with Pyridinium Electron Acceptor Groups, Acc. Chem. Res. 39 (2006) 383–393, https://doi.org/10.1021/ar050225k.
[46] S. Muhammad, H.-L. Xu, R.-L. Zhong, Z.-M. Su, A.G. Al-Sehemi, A. Irfan, Quantum chemical design of nonlinear optical materials by sp2-hybridized carbon nanomaterials: issues and opportunities, J. Mater. Chem. C. 1 (2013) 5439–5449, https://doi.org/10.1039/C3TC31183J.
[47] M. Blanchard-Desce, V. Alain, P.V. Bedworth, S.R. Marder, A. Fort, C. Runser, M. Barzoukas, S. Lebus, R. Wortmann, Large Quadratic Hyperpolarizabilities with Donor–Acceptor Polyenes Exhibiting Optimum Bond Length Alternation: Correlation Between Structure and Hyperpolarizability, Chem.-A Eur. J. 3 (1997) 1091–1104, https://doi.org/10.1002/chem.19970030717.
[48] J.P. Perdew, A. Ruzsinszky, G.I. Csonka, O.A. Vydrov, G.E. Scuseria, L.A. Constantin, X. Zhou, K. Burke, Restoring the Density-Gradient Expansion for Exchange in Solids and Surfaces, Phys. Rev. Lett. 100 (2008) 136406, , https://doi.org/10.1103/PhysRevLett. 100.136406.
[49] F. Ma, Z.-J. Zhou, Z.-R. Li, D. Wu, Y. Li, Z.-S. Li, Lithium salt of end-substituted nanotube: Structure and large nonlinear optical property, Chem. Phys. Lett. 488 (2010) 182–186, https://doi.org/10.1016/j.cplett.2010.02.012.
[50] G. Kresse, J. Hafner, Ab initio molecular dynamics for liquid metals, Phys. Rev. B. 47 (1993) 558–561, https://doi.org/10.1103/PhysRevB.47.558.
[51] H.J. Monkhorst, J.D. Pack, Special points for Brillouin-zone integrations, Phys. Rev. B. 13 (1976) 5188–5192, https://doi.org/10.1103/PhysRevB.13.5188.
[52] E.D. Glendening, A.E. Reed, J.E. Carpenter, F. Weinhold, NBO Version 3.1, NBO Version 3.1.
[53] J.E. Carpenter, F. Weinhold, Analysis of the geometry of the hydroxymethyl radical by the “different hybrids for different spins” natural bond orbital procedure, J. Mol. Struct. Theochem. 169 (1988) 41–62, https://doi.org/10.1016/0166-1280(88)80248-3.
[54] D.Y. Zubarev, A.I. Boldyrev, Developing paradigms of chemical bonding: Adaptive natural density partitioning, Phys. Chem. Chem. Phys. 10 (2008) 5207–5217, https://doi.org/10.1039/b804083d.
[55] D.Y. Zubarev, A.I. Boldyrev, Revealing Intuitively Assessable Chemical Bonding Patterns in Organic Aromatic Molecules via Adaptive Natural Density Partitioning, J. Org. Chem. 73 (2008) 9251–9258, https://doi.org/10.1021/jo801407e.
[56] T.R. Galeev, B.D. Dunnington, J.R. Schmidt, A.I. Boldyrev, Solid state adaptive natural density partitioning: a tool for deciphering multi-center bonding in periodic systems, Phys. Chem. Chem. Phys. 15 (2013) 5022–5029, https://doi.org/10.1039/C3CP50350J.
[57] N.V. Tkachenko, D. Steglenko, N. Fedik, N.M. Boldyreva, R.M. Minyaev, V.I. Minkin, A.I. Boldyrev, Superoctahedral two-dimensional metallic boron with peculiar magnetic properties, Phys. Chem. Chem. Phys. 21 (2019) 19764–19771, https://doi.org/10.1039/c9cp03786a.
[58] N. Fedik, A.I. Boldyrev, Insight into the Nature of Rim Bonds in Coronene, J. Phys. Chem. A. 122 (2018) 8585–8590, https://doi.org/10.1021/acs.jpca.8b07937.
[59] O.A. Gapurenko, R.M. Minyaev, N.S. Fedik, V.V. Koval, A.I. Boldyrev, V.I. Minkin, Structure and bonding of new boron and carbon superpolyhedra, Struct. Chem. 30 (2019) 805–814, https://doi.org/10.1007/s11224-019-1279-5.
[60] N. Fedik, A. Boldyrev, A. Muñoz-Castro, Aromatic Character of $[Au_{13}]^{5+}$ and $[MAu_{12}]^{4+/6+}$ (M = Pd, Pt) Core in Ligand Protected Gold Nanoclusters. Interplay Between Spherical and Planar σ-Aromatics, Phys. Chem. Chem. Phys. (2019) 25215–25219, https://doi.org/10.1039/c9cp04477a.
[61] G. Liu, N. Fedik, C. Martinez-Martinez, S.M. Ciborowski, X. Zhang, A.I. Boldyrev, K.H. Bowen, Realization of Lewis Basic Sodium Anion in the $NaBH_3^-$ Cluster, Angew. Chem.-Int. Ed. 58 (2019) 13789–13793, https://doi.org/10.1002/anie.201907089.
[62] J. Czekner, L.F. Cheung, G.S. Kocheril, M. Kulichenko, A.I. Boldyrev, L.S. Wang, High-Resolution Photoelectron Imaging of IrB_3^-: Observation of a π-Aromatic B_3^+ Ring Coordinated to a Transition Metal, Angew. Chem.-Int. Ed. 58 (2019) 8877–8881, https://doi.org/10.1002/anie.201902406.
[63] M. Kulichenko, N. Fedik, A. Munoz-Castro, A.I. Boldyrev, Expansion of aromaticity magnetic criteria on multi-layer structures. Magnetic response and spherical aromaticity of Matryoshka-like $[Sn@Cu_{12}@Sn_{20}]^{12-}$ cluster, Chem.-A. Eur. J. (2019), https://doi.org/10.1039/c6ra06833b.
[64] M. Kulichenko, N. Fedik, K.V. Bozhenko, A.I. Boldyrev, Hydrated Sulfate Clusters $SO_4^{2-}(H_2O)_n$ (n = 1–40): Charge Distribution Through Solvation Shells and

Stabilization, J. Phys. Chem. B. 123 (2019) 4065–4069, https://doi.org/10.1021/acs.jpcb.9b01744.
[65] N. Fedik, M. Kulichenko, A.I. Boldyrev, Two names of stability: Spherical aromatic or superatomic intermetalloid cluster $[Pd_3Sn_8Bi_6]^{4-}$, Chem. Phys. 522 (2019) 134–137, https://doi.org/10.1016/j.chemphys.2019.02.015.
[66] T.H. Dunning, Gaussian basis sets for use in correlated molecular calculations. I. The atoms boron through neon and hydrogen, J. Chem. Phys. 90 (1989) 1007–1023, https://doi.org/10.1063/1.456153.
[67] A. Togo, F. Oba, I. Tanaka, First-principles calculations of the ferroelastic transition between rutile-type and $CaCl_2$-type SiO_2 at high pressures, Phys. Rev. B. 78 (2008) 134106, , https://doi.org/10.1103/PhysRevB.78.134106.
[68] G.J. Martyna, M.L. Klein, M. Tuckerman, Nosé-Hoover chains: The canonical ensemble via continuous dynamics, J. Chem. Phys. 97 (1992) 2635–2643, https://doi.org/10.1063/1.463940.
[69] X. Gonze, J.-M. Beuken, R. Caracas, F. Detraux, M. Fuchs, G.-M. Rignanese, L. Sindic, M. Verstraete, G. Zerah, F. Jollet, M. Torrent, A. Roy, M. Mikami, P. Ghosez, J.-Y. Raty, D.C. Allan, First-principles computation of material properties: the ABINIT software project, Comput. Mater. Sci. 25 (2002) 478–492, https://doi.org/10.1016/S0927-0256(02)00325-7.
[70] S. Sharma, C. Ambrosch-Draxl, Second-Harmonic Optical Response from First Principles, Phys. Scr. T109 (2004) 128, https://doi.org/10.1238/physica.topical.109a00128.
[71] S. Baroni, S. de Gironcoli, A. Dal Corso, P. Giannozzi, Phonons and related crystal properties from density-functional perturbation theory, Rev. Mod. Phys. 73 (2001) 515–562, https://doi.org/10.1103/RevModPhys. 73.515.
[72] A. Seidl, A. Görling, P. Vogl, J.A. Majewski, M. Levy, Generalized Kohn-Sham schemes and the band-gap problem, Phys. Rev. B. 53 (1996) 3764–3774, https://doi.org/10.1103/PhysRevB.53.3764.
[73] G. Onida, L. Reining, A. Rubio, Electronic excitations: density-functional versus many-body Green's-function approaches, Rev. Mod. Phys. 74 (2002) 601–659, https://doi.org/10.1103/RevModPhys. 74.601.
[74] F. Aryasetiawan, O. Gunnarsson, TheGWmethod, Reports, Prog. Phys. 61 (1998) 237–312, https://doi.org/10.1088/0034-4885/61/3/002.
[75] T.H. Fischer, J. Almlof, General methods for geometry and wave function optimization, J. Phys. Chem. 96 (1992) 9768–9774, https://doi.org/10.1021/j100203a036.
[76] F. Jollet, M. Torrent, N. Holzwarth, Generation of Projector Augmented-Wave atomic data: A 71 element validated table in the XML format, Comput. Phys. Commun. 185 (2014) 1246–1254, https://doi.org/10.1016/j.cpc.2013.12.023.
[77] K. Lejaeghere, G. Bihlmayer, T. Björkman, P. Blaha, S. Blügel, V. Blum, D. Caliste, I.E. Castelli, S.J. Clark, A. Dal Corso, S. de Gironcoli, T. Deutsch, J.K. Dewhurst, I. Di Marco, C. Draxl, M. Dułak, O. Eriksson, J.A. Flores-Livas, K.F. Garrity, L. Genovese, P. Giannozzi, M. Giantomassi, S. Goedecker, X. Gonze, O. Grånäs, E.K.U. Gross, A. Gulans, F. Gygi, D.R. Hamann, P.J. Hasnip, N.A.W. Holzwarth, D. Iuşan, D.B. Jochym, F. Jollet, D. Jones, G. Kresse, K. Koepernik, E. Küçükbenli, Y.O. Kvashnin, I.L.M. Locht, S. Lubeck, M. Marsman, N. Marzari, U. Nitzsche, L. Nordström, T. Ozaki, L. Paulatto, C.J. Pickard, W. Poelmans, M.I.J. Probert, K. Refson, M. Richter, G.-M. Rignanese, S. Saha, M. Scheffler, M. Schlipf, K. Schwarz, S. Sharma, F. Tavazza, P. Thunström, A. Tkatchenko, M. Torrent, D. Vanderbilt, M.J. van Setten, V. Van Speybroeck, J.M. Wills, J.R. Yates, G.-X. Zhang, S. Cottenier, Reproducibility in density functional theory calculations of solids, Science 351 (2016) aad3000, https://doi.org/10.1126/science.aad3000.
[78] J.Y. Lim, J.S. Oh, B.D. Ko, J. Won Cho, S.O. Kang, G. Cho, H.S. Uhm, E.H. Choi, Work function of MgO single crystals from ion-induced secondary electron emission coefficient, J. Appl. Phys. 94 (2003) 764–769, https://doi.org/10.1063/1.1581376.
[79] D.M. Roessler, W.C. Walker, Electronic Spectrum and Ultraviolet Optical Properties of Crystalline MgO, Phys. Rev. 159 (1967) 733–738, https://doi.org/10.1103/PhysRev. 159.733.
[80] J.P. Perdew, K. Burke, M. Ernzerhof, Generalized gradient approximation made simple, Phys. Rev. Lett. 77 (1996) 3865–3868, https://doi.org/10.1103/PhysRevLett. 77.3865.
[81] J. Heyd, G.E. Scuseria, M. Ernzerhof, Hybrid functionals based on a screened Coulomb potential, J. Chem. Phys. 118 (2003) 8207–8215, https://doi.org/10.1063/1.1564060.
[82] J. Heyd, G.E. Scuseria, M. Ernzerhof, Erratum: "Hybrid functionals based on a screened Coulomb potential" [J. Chem. Phys. 118, 8207 (2003)], J. Chem. Phys. 124 (2006) 219906, https://doi.org/10.1063/1.2204597.
[83] J.L.P. Hughes, J.E. Sipe, Calculation of second-order optical response in semiconductors, Phys. Rev. B. 53 (1996) 10751–10763, https://doi.org/10.1103/PhysRevB.53.10751.
[84] J.L.P. Hughes, Y. Wang, J.E. Sipe, Calculation of linear and second-order optical response in wurtzite GaN and AlN, Phys. Rev. B. 55 (1997) 13630–13640, https://doi.org/10.1103/PhysRevB.55.13630.
[85] J.E. Sipe, A.I. Shkrebtii, Second-order optical response in semiconductors, Phys. Rev. B. 61 (2000) 5337–5352, https://doi.org/10.1103/PhysRevB.61.5337.
[86] C.B. Huang, Z.Y. Wang, H.X. Wu, Y.B. Ni, R.C. Xiao, M. Qi, Ab initio study of the linear and nonlinear optical properties of hexagonal CdSe, Comput. Condens. Matter. 3 (2015) 41–45, https://doi.org/10.1016/j.cocom.2015.02.002.
[87] S.N. Rashkeev, S. Limpijumnong, W.R.L. Lambrecht, Second-harmonic generation and birefringence of some ternary pnictide semiconductors, Phys. Rev. B. 59 (1999) 2737–2748, https://doi.org/10.1103/PhysRevB.59.2737.
[88] M.-Z. Huang, W.Y. Ching, Calculation of optical excitations in cubic semiconductors. I. Electronic structure and linear response, Phys. Rev. B. 47 (1993) 9449–9463, https://doi.org/10.1103/PhysRevB.47.9449.
[89] N. Pavliček, A. Mistry, Z. Majzik, N. Moll, G. Meyer, D.J. Fox, L. Gross, Synthesis and characterization of triangulene, Nat. Nanotechnol. 12 (2017) 308.
[90] L. Gross, F. Mohn, N. Moll, P. Liljeroth, G. Meyer, The Chemical Structure of a Molecule Resolved by Atomic Force Microscopy, Science 325 (2009), https://doi.org/10.1126/science.1176210 1110 LP–1114.
[91] L. Gross, F. Mohn, N. Moll, B. Schuler, A. Criado, E. Guitián, D. Peña, A. Gourdon, G. Meyer, Bond-Order Discrimination by Atomic Force Microscopy, Science 337 (2012), https://doi.org/10.1126/science.1225621 1326 LP–1329.
[92] N. Pavliček, B. Schuler, S. Collazos, N. Moll, D. Pérez, E. Guitián, G. Meyer, D. Peña, L. Gross, On-surface generation and imaging of arynes by atomic force microscopy, Nat. Chem. 7 (2015) 623.
[93] B. Schuler, S. Fatayer, F. Mohn, N. Moll, N. Pavliček, G. Meyer, D. Peña, L. Gross, Reversible Bergman cyclization by atomic manipulation, Nat. Chem. 8 (2016) 220.